

Pressure-induced phase transitions of exposed curved surface nano-TiO₂ with high photocatalytic activity

Yanwei Huang, Fengjiao Chen, Xin Li, Ye Yuan, Haini Dong, Sudeshna Samanta, Zhenhai Yu, Saqib Rahman, Jun Zhang, Ke Yang, Shuai Yan, and Lin Wang

Citation: *Journal of Applied Physics* **119**, 215903 (2016); doi: 10.1063/1.4953218

View online: <http://dx.doi.org/10.1063/1.4953218>

View Table of Contents: <http://scitation.aip.org/content/aip/journal/jap/119/21?ver=pdfcov>

Published by the [AIP Publishing](#)

Articles you may be interested in

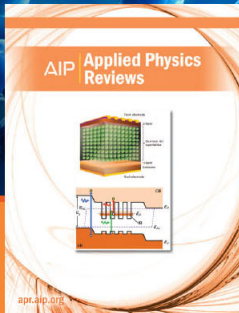
[Augmented photocatalytic activity and luminescence response of Tb³⁺ doped nanoscale titania systems](#)
J. Appl. Phys. **116**, 144902 (2014); 10.1063/1.4897369

[Enhancement of optical absorption by modulation of the oxygen flow of TiO₂ films deposited by reactive sputtering](#)
J. Appl. Phys. **111**, 113513 (2012); 10.1063/1.4724334

[Investigation of photocatalytic activity of TiO₂/WO₃ bilayered thin films with various amounts of WO₃ exposed surface](#)
J. Vac. Sci. Technol. A **27**, 880 (2009); 10.1116/1.3086647

[Effect of nitrogen on the photocatalytic activity of TiO_xN_y thin films](#)
J. Vac. Sci. Technol. A **24**, 1156 (2006); 10.1116/1.2174018

[Degradation in photocatalytic activity induced by hydrogen-related defects in nano- LiNbO₃ material](#)
Appl. Phys. Lett. **88**, 071917 (2006); 10.1063/1.2175479



NEW Special Topic Sections

NOW ONLINE
Lithium Niobate Properties and Applications:
Reviews of Emerging Trends

AIP | Applied Physics Reviews

Pressure-induced phase transitions of exposed curved surface nano-TiO₂ with high photocatalytic activity

Yanwei Huang,^{1,2,a)} Fengjiao Chen,¹ Xin Li,¹ Ye Yuan,¹ Haini Dong,^{1,4} Sudeshna Samanta,¹ Zhenhai Yu,¹ Saqib Rahman,¹ Jun Zhang,² Ke Yang,³ Shuai Yan,³ and Lin Wang^{1,a)}

¹Center for High Pressure Science and Technology Advanced Research, Shanghai 201203, China

²College of Materials and Environmental Engineering, Hangzhou Dianzi University, Hangzhou 310018, China

³Shanghai Synchrotron Radiation Facility (SSRF), Shanghai Institute of Applied Physics, Chinese Academy of Science, Shanghai 201800, China

⁴Key Laboratory of High-Temperature and High-Pressure Study of the Earth's Interior, Institute of Geochemistry, Chinese Academy of Science, Guiyang, Guizhou 550081, China

HPSTAR
2016-209

(Received 29 February 2016; accepted 21 May 2016; published online 6 June 2016)

We report a unique phase transition in compressed exposed curved surface nano-TiO₂ with high photocatalytic activity using *in situ* synchrotron X-ray diffraction and Raman Spectroscopy. High-pressure studies indicate that the anatase phase starts to transform into baddeleyite phase upon compression at 19.4 GPa, and completely transforms into the baddeleyite phase above 24.6 GPa. Upon decompression, the baddeleyite phase was maintained until the pressure was released to 6.4 GPa and then transformed into the α -PbO₂ phase at 2.7 GPa. Together with the results of high-resolution transmission electron microscopy and the pressure-volume relationship, this phase transition's characteristics during the compression-decompression cycle demonstrate that the truncated biconic morphology possessed excellent stability. This study may provide an insight to the mechanisms of stability for high photocatalytic activity of nano-TiO₂. *Published by AIP Publishing.*

[<http://dx.doi.org/10.1063/1.4953218>]

I. INTRODUCTION

Various anatase TiO₂ nanostructures have attracted much attention because of their potential applications in photocatalysts,^{1,2} photovoltaic cells,³ water photocatalysts,⁴⁻⁶ and lithium ion batteries.⁷⁻⁹ The performance of different forms of anatase nano-TiO₂ is highly dependent on its size, shape, and exposed crystal facets.¹⁰⁻¹² Studies have shown that the {001} facets of anatase TiO₂ are more reactive than other facets. However, the {001} facets usually diminish rapidly during the crystal nucleation and growth as a result of the minimization of surface energy: {001} 0.90 J/m² > {100} 0.53 J/m² > {101} 0.44 J/m². Nowadays, there are enormous reports in controlling the growth of anatase TiO₂ crystal facets due to the interesting facet-dependent physicochemical properties.¹³⁻¹⁵ A lot of research focuses on how to increase the percentage of the exposed {001} facet and then improve the activities of the photocatalysts. Yang *et al.*¹⁶ reported on the basis of theoretical predictions they synthesized successfully uniform anatase TiO₂ single crystal with a high percentage of {001} facets using hydrofluoric acid as a morphology controlling agent and the performances were enhanced. Sofianou *et al.*¹⁷ reported TiO₂ anatase nanoplates and hollow microspheres with large percentage of the {001} crystal facets, which was successfully fabricated by a solvothermal-hydrothermal method. The photoactivity of these nanoplates is much higher than that of the TiO₂ nanotubes. In addition, 3D hierarchical structures composed of single-crystalline anatase TiO₂ nanosheets dominated by

well-defined {001} facets imply potential applications in dye-sensitized solar cells and photocatalytic areas.¹⁸ However, anatase TiO₂ nanosheets can only absorb UV light with a wavelength of no longer than 387 nm due to the large band gap of 3.2 eV. Thus, to fabricate non-metal-doped (e.g., N-, S-, B-, C-doped) anatase TiO₂ sheets with exposed {001} facets can be a more effective approach to improve the photocatalytic activity. Further, Zhang *et al.*⁶ reported a one-step route to obtain Mo + N codoped TiO₂ sheets with dominant {001} facets by a hydrothermal process using TiN, MoO₃, HF, and HNO₃ as precursor. The Mo + N codoped TiO₂ sheets showed the highest photocatalyst activity when the Mo-doping ratio reached 1%, indicating an appropriate doping ratio is necessary for synergistic effect between doped metal and nonmetal elements. These studies indicate that all the properties of TiO₂ nanostructures highly depend on their crystal structure and specially exposed facets. Functional anatase nanostructured materials, tuned in size or shape, have enhanced photocatalytic effect. Systemically investigated structure and exposed facets evolution process will provide a new insight to illustrate the work mechanism.

Recently, a new class of crystal surface of TiO₂ was obtained which is enclosed by quasi-continuous high-index microfacets and thus has a unique truncated biconic morphology.^{19,20} The biconical facets are curved and the truncated flat facets are {001}. In nature, crystals with curved external surface usually exhibit unique performances, such as stability, elasticity, and electronic and optical properties. For anatase TiO₂ crystal, the equilibrium shape built through Wulff construction is a slightly truncated tetragonal bipyramid enclosed by eight thermodynamically stable {101} facets and two {001} facets. Understanding the mechanism of

^{a)}Authors to whom correspondence should be addressed. Electronic addresses: yanwei.huang@hpstar.ac.cn and wangling@hpstar.ac.cn

crystal structure changes, crystal growth mechanism, exposed facets percentage, and electronic structures that the different polymorphs demonstrate, helps us to master the crystal shape evolution. The change of atomic structure affects the crystal structures and thus external micro-morphology. Pressure is one of the state parameters which can provide a clean way to tune interatomic distances and hence the formation of new structural properties. In recent years, high-pressure techniques have been employed to study the stabilities and structural transitions of TiO₂ nanomaterials to explore its potential application in material science. Some studies have reported that the high pressure behaviors of TiO₂ nanomaterials intensively depend on both the sizes and morphologies of the starting materials. For instance, a unique size-dependent phase transition selectivity under high pressure exists in nanocrystalline anatase TiO₂.^{21–23} In addition, the morphology-dependent phase transitions of anatase TiO₂ presented different phase processes. Morphology-tuned and pressure-driven phase transition of TiO₂ have been observed widely; for example, in nanowires, nanoporous, nanorods, and nanobelts.^{24–26} However, to the best of our knowledge, there is almost no high pressure studies on exposed curved surface nano-TiO₂. Investigating its unique phase transition processes and sequences due to the finite-size limit effect and special nanostructures is an interesting research topic that will provide comprehensive information for the family of TiO₂ nanostructured materials. Thus, in this paper, we report the unique pressure-induced phase transitions of exposed curved surface nano-TiO₂ using *in situ* synchrotron X-ray diffraction (XRD) and Raman spectroscopy in diamond anvil cells (DACs) at room temperature.

II. EXPERIMENTAL DETAILS

The exposed curved facets nano-TiO₂ with high photocatalytic activity was synthesized by a one-step hydrothermal route using tetrabutyl titanate (Ti(OC₄H₉)₄), citric acid, HF (40%), and deionized water as precursor.²⁰ In the concrete process, 25 ml Ti(OC₄H₉)₄ was mixed with relative citric acid, HF, and deionized water in a Teflon-lined autoclave with a capacity of 100 ml then kept at 180 °C for 24 h. The precipitates were then separated from the suspension by centrifugation (4000 rpm, 15 min). The products were further suspended and centrifuged in absolute ethanol three times, followed by drying under an infrared lamp. Then the final powders were calcined at 600 °C for 90 min to clear surface fluoride. The optimal samples of exposed curved surface nano-TiO₂ were obtained at 23 mmol citric acid, 2 ml HF, and 3 ml deionized water, with the mole ratio of citric acid and HF of 1:2. This obtained nano-TiO₂ shows higher photocatalytic activity than that of the TiO₂ nanosheets with exposed {001} facets which confirms the curved surface has higher activity than {001} facets.²⁰ High pressure XRD experiments were performed at the 15U1 beamline of the Shanghai Synchrotron Radiation Facility (SSRF). The incident wavelength of the beam is 0.6199 Å with a beam size of $2 \times 7 \mu\text{m}^2$. The high pressure measurements were carried out at room temperature by using a gasketed high pressure DAC. To produce a quasi-hydrostatic environment around sample,

we used silicone oil as a pressure transmitting medium. Pressure was determined by the pressure dependent spectral shift of the sharp ruby fluorescence R1 line.^{6,27} The sample was placed in a stainless steel gasket hole 150 μm in diameter with the diamond culet size of 500 μm in diameter. High pressure Raman scattering measurements were performed using a Renishaw inVia Raman spectrometer with an excitation wavelength of 532 nm. Morphologies of the samples were characterized by high resolution transmission electron microscopy (HRTEM) which confirmed the unique truncated biconic morphology for nano-TiO₂, as shown in Fig. 1.

III. RESULTS AND DISCUSSION

Fig. 2 shows the pressure evolution of synchrotron XRD patterns for exposed curved surface nano-TiO₂ in the anatase phase upon compression (a) and decompression (b). The diffraction peaks identified in the starting structure were consistent with the diffraction planes of tetragonal anatase TiO₂, agreeing with the JCPDS file No. 21-1272. During compression, shown in Fig. 2(a), the anatase phase was found to

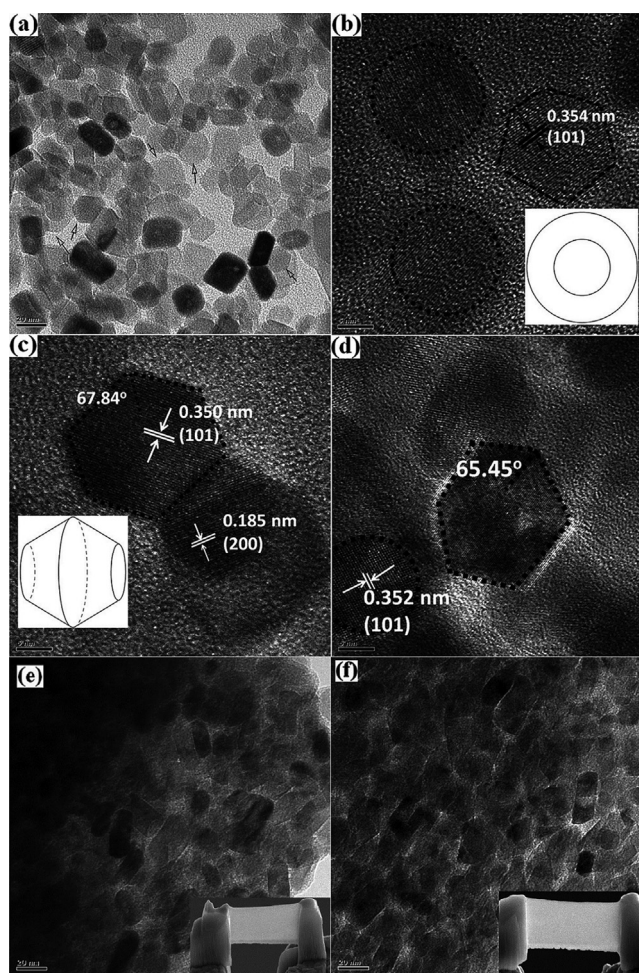


FIG. 1. HRTEM images of exposed curved surface nano-TiO₂. (a) The overall view of the as-prepared nano-TiO₂, and the clear edges and angles were marked by arrows. (b)–(d) High-magnification TEM images were viewed from various orientations, and unique truncated biconic morphology was confirmed. (e) and (f) The quenched nano-TiO₂ from 18 GPa and 36 GPa, and the insets show that the samples have been cut into thinner ones by focused ion beam (FIB) convenient for TEM performance.

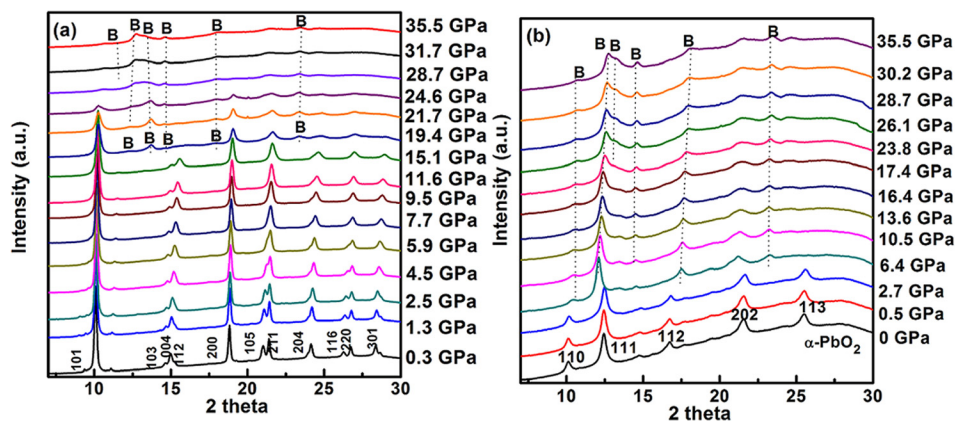


FIG. 2. Synchrotron XRD patterns of exposed curved surface nano-TiO₂ under high pressure: (a) compression and (b) decompression.

persist to 15.1 GPa. At 19.4 GPa, the peaks of (004), (103), and (112) for the anatase phase disappeared and some peaks (marked with B), belonging to a baddeleyite phase, appeared indicating that the anatase phase starts to transform into a baddeleyite structure. With further increasing pressure, the broadening of diffraction peaks such as (101), (200), (211), and (204) for the anatase phase became more obvious and the intensity of these peaks weakened significantly. Above 24.6 GPa, the anatase phase transformed into the baddeleyite structure completely. The peaks for the baddeleyite phase shifted to a high diffraction angle with increasing pressure, indicating the reduction of d-spacing or shrinkage of the unit cells. The weakening intensity of the baddeleyite phase peaks implied a low-ordered structure and partial amorphous phase forming. Until the maximum pressure of 35.5 GPa, the baddeleyite phase still existed with weakened and broadened peaks and we did not observe complete amorphization. Upon decompression (shown in Fig. 2(b)), the high pressure baddeleyite phase was retained until the pressure was released to 6.4 GPa and then transformed into the α -PbO₂ phase at 2.7 GPa.

These results clearly demonstrated that the exposed curved surface nano-TiO₂ transformed directly from anatase to baddeleyite without passage via the α -PbO₂ intermediate. However, upon pressure release to ambient condition, the high pressure baddeleyite phase is quenched to the α -PbO₂ phase, not to the original anatase structure, which is similar to the previous reports.^{22,28} Arlt *et al.*²⁹ believed the direct transition from the anatase to baddeleyite structure was induced by lattice defects and grain boundaries. Hearne *et al.*²⁸ studied the effect of grain size on structural transitions in anatase TiO₂. Based on their calculations from the Raman spectroscopy, they argued that α -PbO₂ phase intermediate will only nucleate and grow as a stable particle if it has a diameter larger than the critical value and that the high pressure phase behaves in a similar way under decompression. Thus, we can infer that the exposed curved nano-TiO₂ aggregates by means of the Vander Waals interaction at the beginning. As the sample pressure is increased and pressurized, its density is supposed to increase when the loose grains pack together. This can change the interfaces, grain boundaries, and further the total surface free energy. There must be a condition of nucleation and growth which some phases satisfied can form. Li³⁰ reported the pressure-induced

phase transitions of TiO₂ nanosheet with exposed {001} facets (the side length 20–40 nm) and they found that the anatase phase persisted to 12.3 GPa, started to transform into the baddeleyite structure at 14.6 GPa and transformed completely into the baddeleyite phase above 22.8 GPa. For the exposed curved surface TiO₂ in this paper, the phase transition pressure is higher, with a gap of about 3 GPa, as both phases experience similar transitions. However, for anatase TiO₂ nanowires (with the diameter size 50–200 nm), the transition from the anatase phase to a baddeleyite structure starts at \sim 9 GPa and transforms completely into baddeleyite phase above 21 GPa. This indicates that the different size and morphologies can influence the transition process, especially the phase transition pressure, and the sample with a larger size has the lower transition pressure. It has been verified that the nanosize materials have higher transition pressures than their corresponding bulk materials.^{31–33}

The phase transition diagrams of bulk and nano-TiO₂ under high pressure are summarized in Fig. 3 and compare this work with previous studies. Fig. 3 shows that the phase transition pressure corresponding to the bulk,²⁸ nanoporous,³⁸ nanowires,²⁶ nanotubes,³⁵ nanosheets,³⁰ and is different in our data. The bulk TiO₂ in anatase phase follows the phase transition route: anatase phase to columbite

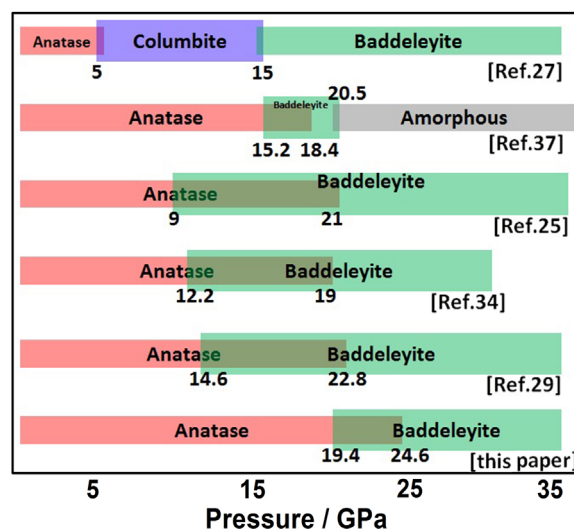


FIG. 3. Phase diagram of bulk and nano-TiO₂ with increasing pressure referred from several adapted literatures.

(orthorhombic α -PbO₂ phase) and then to baddeleyite. However, TiO₂ nanomaterials demonstrate a different phase transition route: the anatase phase transforms to the baddeleyite phase directly, which heavily depends on the sizes and morphologies of nanomaterials. As previously discussed, the phase transition pressure in the exposed curved surface TiO₂ we observed is higher, with a gap of about 3 GPa, which can be attributed to its unique truncated bionic morphology and nanosize grains.

Fig. 4(a) shows the pressure dependence of relative lattice parameters ($a/a_0, c/c_0$) of exposed curved surface nano-TiO₂ in the range of 0–15.1 GPa. It shows that the c -axis length is more compressible than the a -axis length, due to the difference in the directional population of the hard occupied (TiO₆) and soft empty (O₆) oxygen octahedral.²⁶ This is consistent with the properties of previously reported anatase nanowires, nanosheets, nanoparticles and bulks.^{26,30,34} The reduction in the size of the grains can block the compressibility tendency. However, until the phase transition appears, the c -axis is more highly compressible than the a or b axis for the anatase phase, regardless of the microphology or exposed facets changes. Fig. 4(b) shows the pressure dependence of the volume. The pressure-volume data for the nano-

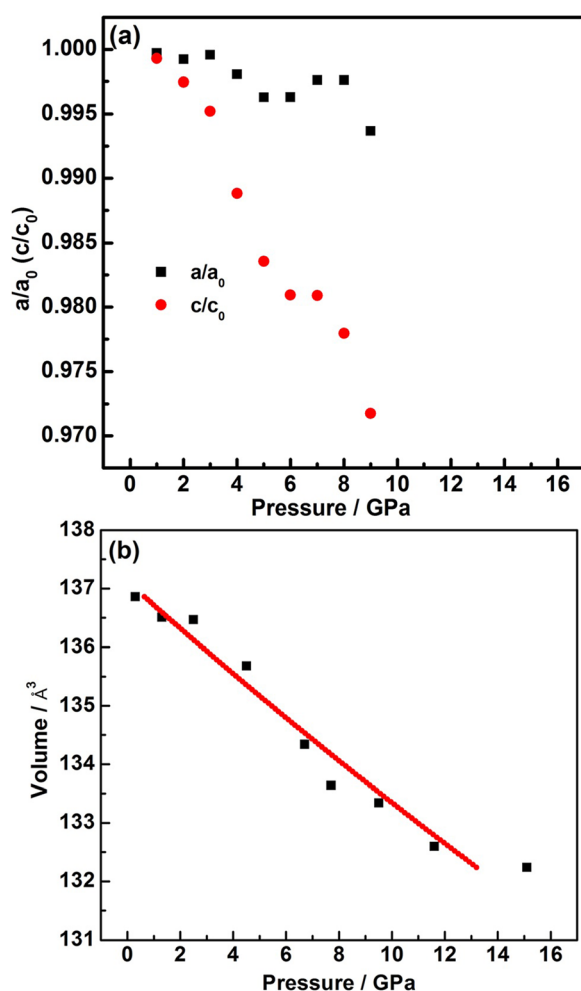


FIG. 4. The pressure dependence of relative lattice parameters ($a/a_0, c/c_0$) (a) and the pressure-volume diagram (b) of exposed curved surface nano-TiO₂.

TiO₂ was fitted to the third-order Birch-Murnaghan equation of state³⁵

$$P(V) = 1.5B_0 \left[\left(\frac{V_0}{V} \right)^{\frac{7}{3}} - \left(\frac{V_0}{V} \right)^{\frac{5}{3}} \right] \times \left\{ 1 + \frac{3}{4}(B_0' - 4) \left[\left(\frac{V_0}{V} \right)^{\frac{2}{3}} - 1 \right] \right\}.$$

The bulk modulus (B_0) was determined at 338.81 GPa with the first derivative (B_0') fixed at 4. The bulk modulus is much higher than those of the nanoparticles (180–240 GPa),^{23,29,30,36,37} rice-shape nanoparticles (319 GPa),³⁴ and nanosheets (317 GPa).³⁰ This indicated that this nano-TiO₂ is more incompressible than other morphological TiO₂. The incompressibility can be ascribed to the nanosize effects and special exposed curved facets.

Fig. 5 shows the Raman spectra of exposed curved surface nano-TiO₂ during compression (a) and decompression (b). In Fig. 5(a), at 1.2 GPa pressure, there are almost five Raman active modes observed at 149 cm⁻¹(E_g), 399 cm⁻¹(B_{1g}), 515 cm⁻¹(A_{1g} and B_{1g}), and 641 cm⁻¹(E_g), which agree with the TiO₂ anatase structure in previous reports.^{23,30,38} With increasing pressure, the Raman peak 399 cm⁻¹(E_g) disappeared at 15 GPa, and all the other Raman bands showed blue-shift, becoming weaker and broader. When the pressure reached 17.8 GPa, an additional Raman band at 495 cm⁻¹ occurred, which can be attributed to the appearance of the baddeleyite phase. This is basically consistent with the result of XRD, where the phase transition appeared. However, the intensity of the baddeleyite phase decreased gradually with increasing pressure up to 31.2 GPa, which revealed that the nano-TiO₂ was composed of a disordered structure and partial amorphization. Upon decompression, the intensity of the peak of the baddeleyite phase is obvious, until the pressure is released to 8.2 GPa. When the pressure is released to ambient pressure, the baddeleyite phase almost completely transformed into the α -PbO₂ phase, which revealed the quenched sample has the structure of a α -PbO₂ phase. This phase transition was confirmed by the results of synchrotron XRD. Compared to previous reports,^{26,30} the phase transition pressure always lagged behind at about 3 GPa for this biconical nano-TiO₂, in both from the XRD and Raman spectra, which indicated that this material proves more incompressible than other similar nanomaterials. To further study the effect of compression on the change of the grain size, we performed HRTEM on quenched nano-TiO₂. Figs. 1(e) and 1(f) show the TEM images of the samples that were decompressed from 18 GPa and 36 GPa and corresponded to the phase transition pressure and highest pressure reached, respectively. It shows that the average grain size of nano-TiO₂ did not change obviously, except for the increased grain boundary density. The insets in Figs. 1(e) and 1(f) shows the samples have been cut into thinner ones by focused ion beam (FIB) convenient for TEM performance.

As shown in Fig. 6, all four Raman peaks (assigned to two E_g modes, one B_{1g} mode, and one A_{1g}/B_{1g} duplicated mode) shift to higher frequencies under compression. The pressure dependence of the Raman frequencies shift slope

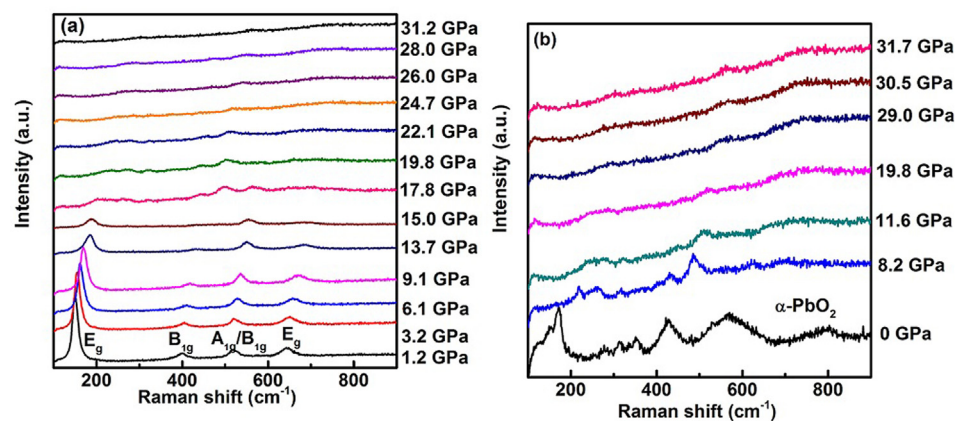


FIG. 5. Raman spectra of the nano-TiO₂ at various pressure: (a) compression and (b) decompression.

have been linearly fitted over the compression. The fitted values that correspond to the peaks of E_g (149 cm⁻¹), B_{1g} (399 cm⁻¹), A_{1g}/B_{1g} (515 cm⁻¹), and E_g (641 cm⁻¹) modes are 2.83 cm⁻¹/GPa (0.09), 2.12 cm⁻¹/GPa (0.16), 2.71 cm⁻¹/GPa (0.11), and 3.25 cm⁻¹/GPa (0.09), respectively. The phase transition occurred at around 17.8 GPa (baddeleyite) and has the pressure coefficient of 3.13 cm⁻¹/GPa. The average slope of the intense E_g band (located at 149 cm⁻¹) is comparable with other anatase nanoparticles (2.58 cm⁻¹/GPa), nanoporous anatase TiO₂ (2.84 cm⁻¹/GPa) and bulks (2.7 cm⁻¹/GPa).^{28,38,39} The slopes can laterally reflect from lateral view the fluctuation of the bulk modulus values.^{22,29,40,41}

IV. CONCLUSIONS

Using exposed curved surface anatase nano-TiO₂ as a starting material, high pressure-driven structural transitions were studied with *in situ* synchrotron radiation and Raman spectroscopy. The results revealed that the exposed curved surface anatase nano-TiO₂ started to transform into the baddeleyite phase upon compression to 19.4 GPa, and completely transformed into the baddeleyite phase above 24.6 GPa, but when the pressure was released to an ambient pressure, the baddeleyite phase completely transformed into

the α -PbO₂ phase. Although other TiO₂ nanomaterials display similar phase transition, the phase transition pressure in this study is higher, with a gap of about 3 GPa. The pressure dependence observed in the Raman spectrum confirms that this exposed curved surface nano-TiO₂ displays higher incompressibility than its other counterparts.

ACKNOWLEDGMENTS

This work was supported by the Program of NSAF (Grant No. U1530402) and the Natural Science Foundation of China (Grant Nos. 10904022 and 61504034). The authors are grateful to Yanjun Li from the Shanghai Institute Measurement and Testing Technology (SIMT) for the HRTEM measurements, and to J. Zhang's group members (Hangzhou Dianzi University) for the synthesized samples.

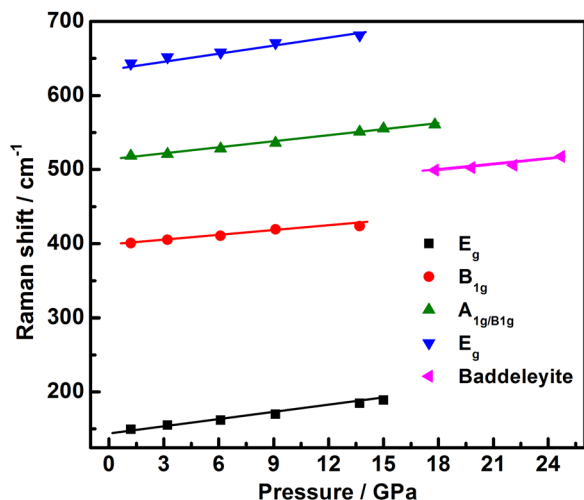


FIG. 6. Pressure dependence of the peak frequencies of Raman spectra for the nano-TiO₂.

- ¹H. Park, W. R. Kim, and H. T. Jeong *et al.*, "Fabrication of dye-sensitized solar cells by transplanting highly ordered TiO₂ nanotube arrays," *Sol. Energy Mater. Sol. Cells* **95**, 184–189 (2011).
- ²H. Zhang, P. Liu, X. Liu *et al.*, "Fabrication of highly ordered TiO₂ nanorod/nanotube adjacent arrays for photoelectrochemical applications," *Langmuir* **26**, 11226–11232 (2010).
- ³K. Shankar, G. K. Mor, and H. E. Prakasam *et al.*, "Self-assembled hybrid polymer-TiO₂ nanotube array heterojunction solar cells," *Langmuir* **23**, 12445–12449 (2007).
- ⁴J. E. G. J. Wijnhoven and W. L. Vos, "Preparation of photonic crystals made of air spheres in titania," *Science* **281**, 802 (1998).
- ⁵J. Yu, Y. Su, and B. Cheng, "Template-free fabrication and enhanced photocatalytic activity of hierarchical macro-/mesoporous titania," *Adv. Funct. Mater.* **17**, 1984 (2007).
- ⁶J. Zhang, J. Xi, and Z. Ji, "Mo + N codoped TiO₂ sheets with dominant {001} facets for enhancing visible-light photocatalytic activity," *J. Mater. Chem.* **22**, 17700 (2012).
- ⁷X. Bai, X. Zhang, and Z. Hua *et al.*, "Uniformly distributed anatase TiO₂ nanoparticles on graphene: Synthesis, characterization, and photocatalytic application," *J. Alloy Compd.* **599**, 10–18 (2014).
- ⁸H. Li, X. Shen, and Y. Liu *et al.*, "Facile phase control for hydrothermal synthesis of anatase-rutile TiO₂ with enhanced photocatalytic activity," *J. Alloy Compd.* **646**, 380–386 (2015).
- ⁹W. Wang, Y. Ni, and Z. Xu, "One-step uniformly hybrid carbon quantum dots with high-reactive TiO₂ for photocatalytic application," *J. Alloys Compd.* **622**, 303–308 (2015).
- ¹⁰Z. C. Lai, F. Peng, and Y. Wang, "Low temperature solvothermal synthesis of anatase TiO₂ single crystals with wholly {100} and {001} faceted surfaces," *J. Mater. Chem.* **22**, 23906–23912 (2012).
- ¹¹T. C. An, J. Y. Chen, and X. Nie *et al.*, "Synthesis of carbon nanotubes-anatase TiO₂ submicron-sized sphere composite photocatalyst for synergistic degradation of gaseous styrene," *ACS Appl. Mater. Interfaces* **4**, 5988–5996 (2012).

- ¹²J. Chen, G. Li, and H. Zhang *et al.*, "Anatase TiO₂ mesocrystals with exposed (001) surface for enhanced photocatalytic decomposition capability toward gaseous styrene," *Catal. Today* **224**, 216–224 (2014).
- ¹³M. M. Maitani, K. Tanaka, and D. Mochizuki *et al.*, "Enhancement of photoexcited charge transfer by {001} facet-dominating TiO₂ nanoparticles," *Phys. Chem. Lett.* **2**, 2655–2659 (2011).
- ¹⁴D. C. Sayle and T. X. T. Sayle, "High-pressure crystallisation of TiO₂ nanoparticles," *J. Comput. Theor. Nanosci.* **4**(2), 299–308 (2007).
- ¹⁵W. Wang, Y. Zhou, and C. Lu *et al.*, "The effect of hydrothermal temperature on the structure and photocatalytic activity of {001} faceted anatase TiO₂," *Mater. Lett.* **160**, 231–234 (2015).
- ¹⁶H. G. Yang, C. H. Sun, and S. Z. Qiao *et al.*, "Anatase TiO₂ single crystals with a large percentage of reactive facets," *Nature* **453**, 638–641 (2008).
- ¹⁷M.-V. Sofianou, C. Trapalis, V. Psycharis, N. Boukos, T. Vaimakis, J. Yu, and W. Wang, "Study of TiO₂ anatase nano and microstructures with dominant {001} facets for NO oxidation," *Environ. Sci. Pollut. Res.* **19**, 3719–3726 (2012).
- ¹⁸W. Qi, Fang, Ji. Z. Zhou, and J. Liu *et al.*, "Hierarchical structures of single-crystalline anatase TiO₂ nanosheets dominated by {001} facets," *Chem. Eur. J.* **17**, 1423–1427 (2011).
- ¹⁹S. Yang, B. X. Yang, and L. Wu *et al.*, "Titania single crystals with a curved surface," *Nat. Commun.* **5**, 5355 (2014).
- ²⁰J. Zhang, Bo. Wu, and L. Huang *et al.*, "Anatase nano-TiO₂ with exposed curved surface for high photocatalytic activity," *J. Alloys Compd.* **661**, 441–447 (2016).
- ²¹M. Nishi, T. Irifune, and J. Tsuchiya *et al.*, "Stability of hydrous silicate at high pressures and water transport to the deep lower mantle," *Nat. Geosci.* **7**, 224–227 (2014).
- ²²V. Swamy, A. Kuznetsov, and L. S. Dubrovinsky, "Finite-size and pressure effects on the Raman spectrum of nanocrystalline anatase TiO₂," *Phys. Rev. B* **71**, 184302 (2005).
- ²³V. Swamy, A. Kuznetsov, and L. S. Dubrovinsky *et al.*, "Size-dependent pressure-induced amorphization in nanoscale TiO₂," *Phys. Rev. Lett.* **96**, 135702 (2006).
- ²⁴V. Swamy, A. Y. Kuznetsov, and L. S. Dubrovinsky *et al.*, "Unusual compression behavior of Anatase TiO₂ nanocrystal," *Phys. Rev. Lett.* **103**, 075505 (2009).
- ²⁵Y. J. Wang, Y. S. Zhao, J. Z. Zhang, and H. W. Xu *et al.*, "In situ phase transition study of nano- and coarse-grained tio₂ under high pressure/temperature conditions," *J. Phys.: Condens. Mater.* **20**, 125224 (2008).
- ²⁶Q. Li, B. Cheng, X. Yang, and R. Liu *et al.*, "Morphology-tuned phase transitions of anatase TiO₂ nanowires under high pressure," *J. Phys. Chem. C* **117**, 8516–8521 (2013).
- ²⁷A. G. Dylla, G. Henkelman, and K. J. Stevenson, "Lithium insertion in nanostructured TiO₂(B) architectures," *Acc. Chem. Res.* **46**, 1104–1112 (2013).
- ²⁸G. R. Heame, J. Zhao, and A. M. Dawe *et al.*, "Effect of grain size on structural transitions in anatase TiO₂: A Raman spectroscopy study at high pressure," *Phys. Rev. B* **70**, 134102 (2004).
- ²⁹T. Arlt, M. Beermejo, and M. A. Blanco *et al.*, "High-pressure polymorphs of anatase TiO₂," *Phys. Rev. B* **61**, 14414 (2000).
- ³⁰Q. Li, B. Cheng, and B. Tian *et al.*, "Pressure-induced phase transitions of TiO₂ nanosheets with high reactive {001} facets," *RSC Adv.* **4**, 12873–12877 (2014).
- ³¹M. J. Bushiri, R. Vinod, A. Segura, and J. A. Sans, "Pressure-induced phase transition in hydrothermally grown ZnO nanoflowers investigated by Raman and photoluminescence spectroscopy," *J. Phys. Condens. Matter* **27**, 385401 (2015).
- ³²L. Wang, W. Yang, Y. Ding, and Y. Ren *et al.*, "Size-dependent amorphization of nanoscale Y₂O₃ at high pressure," *Phys. Rev. Lett.* **105**, 095701 (2010).
- ³³N. Fujisawa, S. Ruffell, J. E. Bradby, J. S. Williams, B. Haberl, and O. L. Warren, "Understanding pressure-induced phase-transformation behavior in silicon through in situ electrical probing under cyclic loading conditions," *J. Appl. Phys.* **105**, 106111 (2009).
- ³⁴S. W. Park, J. T. Jang, and J. Cheon *et al.*, "Shape-dependent compressibility of TiO₂ anatase nanoparticles," *J. Phys. Chem. C* **112**, 9627 (2008).
- ³⁵A. Zhao, "Optical properties, electronic structures and high pressure study of nanostructured one dimensional titanium dioxide by synchrotron radiation and spectroscopy," Electronic Thesis and Dissertation Repository (University of Western Ontario, 2013).
- ³⁶V. Pischedda, G. R. Hearne, and A. M. Dawe, "Ultrastability and enhanced stiffness of ~ 6 nm TiO₂ nanoanatase and eventual pressure-induced disorder on the nanometer scale," *Phys. Rev. Lett.* **96**, 035509 (2006).
- ³⁷Y. Al-Khataatbeh, K. K. M. Lee, and B. Kiefer, "Compressibility of nanocrystalline TiO₂ Anatase," *J. Phys. Chem. C* **116**, 21635 (2012).
- ³⁸Q. Li, R. Liu, and B. Cheng *et al.*, "High pressure behavior of nanoporous anatase TiO₂," *Mater. Res. Bull.* **47**, 1396–1399 (2012).
- ³⁹J. Houska, S. Mraz, and J. M. Schneider, "Experimental and molecular dynamics study of the growth of crystalline TiO₂," *J. Appl. Phys.* **112**, 073527 (2012).
- ⁴⁰V. Swamy, L. S. Dubrovinsky, and N. A. Dubrovinskaia *et al.*, "Compression behavior of nanocrystalline anatase TiO₂," *Solid State Commun.* **125**, 111–115 (2003).
- ⁴¹V. Swamy, J. D. Gale, and L. S. Dubrovinsky, "Atomistic simulation of the crystal structures and bulk moduli of TiO₂ polymorphs," *J. Phys. Chem. Solids* **62**, 887–895 (2001).